Flexible Low-Voltage Organic Complementary Circuits: Finding the Optimum Combination of Semiconductors and Monolayer Gate Dielectrics

Ulrike Kraft, Mirsada Sejfić, Myeong Jin Kang, Kazuo Takimiya, Tarek Zaki, Florian Letzkus, Joachim N. Burghartz, Edwin Weber, and Hagen Klauk*

The organic semiconductor DNTT (dinaphtho-[2,3-b:2′,3′-f]thieno[3,2-b]thiophene)[1] and its didecyl- and diphenyl derivatives C_{10}-DNTT[2] and DPh-DNTT[3] have recently demonstrated great potential for the realization of high-performance p-channel thin-film transistors (TFTs), with charge-carrier mobilities close to 10 cm^2/Vs,[4–6] small parasitic contact resistances[5–7] and exceptional air stability.[3,8] In addition, it has been found that the carrier mobility in vacuum-deposited films of these small-molecule thienoacenes is not significantly affected by the substrate roughness, so that TFTs and circuits based on these semiconductors show excellent performance not only when fabricated on smooth silicon or glass substrates,[1–9] but also when fabricated on much rougher substrates, such as plastic foil,[10–12] printing paper[13] or banknotes.[14] These novel semiconductors therefore show great promise for the realization of flexible, large-area electronics systems, such as sensor arrays and active-matrix displays.

In addition to a large number of individual TFTs that isolate and control the individual sensor or display elements within the active matrix, such applications will also require peripheral integrated circuits, such as row decoders, column drivers and signal converters.[15] In principle, such circuits can be realized in a unipolar design based entirely on p-channel TFTs.[9,16,17] However, in terms of noise margin and power consumption, the integration of p-channel and n-channel TFTs into complementary circuits is expected to provide significant advantages over unipolar circuits.[18,19] But since the performance of even the best organic n-channel TFTs is still notably inferior to that of organic p-channel TFTs, the choice of the semiconductor for the n-channel TFTs in complementary circuits is even more crucial than that for the p-channel TFTs.

Among the very few organic semiconductors that have shown carrier mobilities greater than 1 cm^2/Vs in n-channel TFTs operated in ambient air[20] is the small-molecule material Polyera ActivInk N1100 (PTCDI-$(CN)_2$-$(CH_2C_3F_7)_2$).[21–23] In addition to an exceptionally large electron mobility, N1100 also provides very good long-term stability in ambient air.[24] The N1100 molecule consists of a perylene tetracarboxylic diimide (PTCDI) core equipped with cyano substituents at the bay positions and fluoroalkyl substituents at the imide positions. These strongly electronegative substituents have beneficial effects on the material's packing density, electron mobility and air stability. Interestingly, the largest mobilities reported for thin films of ActivInk N1100 were obtained in TFTs in which the gate-dielectric surface had been modified with a self-assembled monolayer (SAM) based on a fluoroalkyl silane[23] or a fluoroalkyl phosphonic acid[24] prior to the semiconductor deposition. This is unusual, as most organic semiconductors show better performance when deposited onto alkyl SAMs.[25–27] The fact that ActivInk N1100 displays a preference for fluoroalkyl SAMs is possibly related to specific interactions between the fluoroalkyl substituents of ActivInk N1100 and the fluoroalkyl substituents of the gate-dielectric SAM. Such specific interactions between the fluorine substituents of organic semiconductors and SAMs have been observed and discussed previously.[28,29]

Assuming that the semiconductor chosen for the n-channel TFTs shows better performance on fluoroalkyl SAMs than on alkyl SAMs (as mentioned above for ActivInk N1100), while the semiconductor for the p-channel TFTs performs better on alkyl SAMs (as will be shown below for DNTT, DPh-DNTT and C_{10}-DNTT), an interesting question arises, namely which approach regarding the choice of the SAM will provide the highest-performing complementary circuits. An obvious strategy is to modify the gate dielectric of the p-channel TFTs with an alkyl SAM and that of the n-channel TFTs with a fluoroalkyl SAM in order to obtain the best performance for all TFTs, but this requires the selective deposition of different SAMs on the same

U. Kraft, M. Sejfić, Dr. H. Klauk
Max Planck Institute for Solid State Research
Heisenbergstr. 1, 70569, Stuttgart, Germany
E-mail: U.Kraft@fkf.mpg.de
U. Kraft, Prof. E. Weber
Institute for Organic Chemistry
Technical University Freiberg
09596, Freiberg, Germany
Dr. M. J. Kang
Department of Applied Chemistry
Institute for Advanced Materials Research
Hiroshima University
Higashi-Hiroshima, Japan
Prof. K. Takimiya
RIKEN Center for Emergent Matter Science (CEMS)
Wako, Saitama, Japan
T. Zaki, Prof. J. N. Burghartz
Institute for Nano- and Microelectronic Systems
University of Stuttgart, Germany
T. Zaki, Dr. F. Letzkus, Prof. J. N. Burghartz
Institute for Microelectronics
IMS Chips, Stuttgart, Germany

DOI: 10.1002/adma.201403481

© 2014 WILEY-VCH Verlag GmbH & Co. KGaA, Weinheim

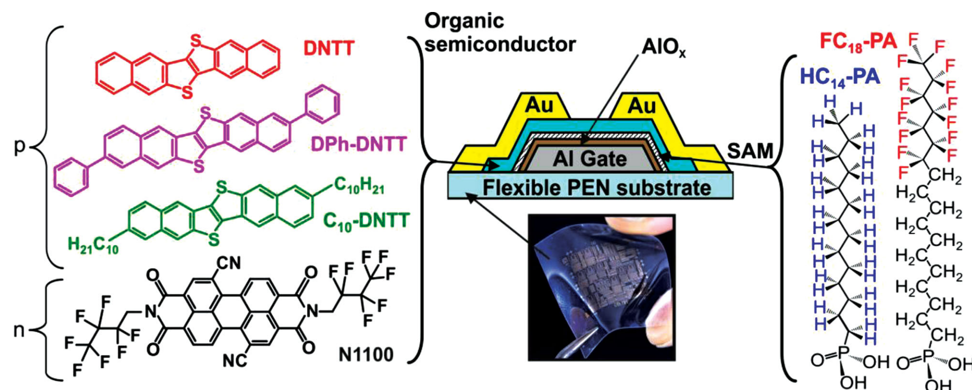

Figure 1. Chemical structures of the organic semiconductors DNTT, DPh-DNTT and C_{10}-DNTT (for the p-channel TFTs) and Polyera ActivInk N1100 (for the n-channel TFTs); schematic cross-section and photograph of the bottom-gate, top-contact (staggered inverted) TFTs fabricated on a flexible polyethylene naphthalate (PEN) substrate; chemical structure of the alkyl- and fluoroalkyl-phosphonic acids (HC_{14}-PA and FC_{18}-PA) utilized for the self-assembled monolayer (SAM) that is part of the ultrathin gate dielectric.

substrate, which is in principle possible,[30] but has certain limitations in terms of the achievable resolution and patterning accuracy.

We have therefore evaluated how the choice of a single gate-dielectric SAM (either alkyl or fluoroalkyl) affects the characteristics of DNTT, DPh-DNTT, C_{10}-DNTT, and N1100 TFTs as well as the switching speed of complementary ring oscillators based on these materials fabricated on flexible polyethylene naphthalate (PEN) substrates and operating at voltages of about 3 V. Given the modest field-effect mobilities in organic TFTs, switching speeds in the megahertz range are possible only by aggressive scaling of the lateral TFT dimensions (channel length and gate-to-contact overlap) to a few microns or even below 1 µm.[7] And since our analysis shows that the compromise regarding the choice of the SAM and the semiconductor is significantly affected by the contact resistance and hence by the channel length of the TFTs, we have varied the channel length of both the p-channel and the n-channel TFTs over a wide range, from 100 µm down to 0.5 µm. For the optimum combination of SAM and semiconductors, a signal propagation delay of 3.1 µs per stage was measured in an 11-stage complementary ring oscillator based on TFTs having a channel length of 1 µm.

A well-studied effect of the SAM functionalization of the gate dielectric of bottom-gate organic TFTs is the resulting difference in the threshold voltage: fluoroalkyl SAMs consistently give more positive threshold voltages than alkyl SAMs. This effect has been observed for various dielectrics and semiconductors[25–27,31,32] and has been ascribed to the built-in electric field generated by the dipole moment of the SAM[25,33] or to a charge transfer between the semiconductor and the SAM/dielectric.[34,35] Since the difference between the threshold voltages of TFTs with alkyl and fluoroalkyl SAMs has been shown to depend on the semiconductor,[27] we have specifically analyzed this SAM-controlled threshold-voltage difference. Performing this analysis over a wide range of channel lengths allows us to check for threshold-voltage roll-off, which is an undesirable short-channel effect that can occur when the channel length is aggressively reduced without appropriate scaling of the gate-dielectric thickness.[36]

The chemical structures of the four organic semiconductors investigated in this study (DNTT, DPh-DNTT, C_{10}-DNTT, N1100) and of the two phosphonic acids utilized for the ultrathin AlO_x/SAM gate dielectric (HC_{14}-PA, FC_{18}-PA) are shown in **Figure 1**, along with the schematic cross-section of the bottom-gate, top-contact TFTs and a photograph of a flexible PEN substrate with a large number of transistors and complementary circuits.

Figure 2a,b shows the measured transfer characteristics of flexible DNTT, DPh-DNTT and C_{10}-DNTT p-channel and N1100 n-channel TFTs with a channel length of 60 µm and with a gate dielectric composed of a 3.6-nm-thick plasma-grown AlO_x layer and a self-assembled monolayer of either the alkyl-phosphonic acid (HC_{14}-PA) or the fluoroalkyl-phosphonic acid (FC_{18}-PA). The effective field-effect mobilities and subthreshold swings of these long-channel TFTs are summarized in **Table 1**. The effect of the choice of the SAM on the threshold voltage of the TFTs is clearly visible: TFTs with the AlO_x/FC_{18}-PA SAM gate dielectric have distinctly more positive threshold voltages than TFTs with the AlO_x/HC_{14}-PA SAM gate dielectric, which is consistent with previous reports of this phenomenon.[25–27,31–35]

Depending on the semiconductor, the difference between the threshold voltage of the TFTs with the fluoroalkyl SAM and that of the TFTs with the alkyl SAM ranges from 1.3 V for N1100 to 1.6 V for DPh-DNTT, 1.7 V for C_{10}-DNTT, and 1.9 V for DNTT (see Figure 2c). These threshold-voltage differences are similar to those previously reported for pentacene p-channel TFTs and F_{16}CuPc n-channel TFTs with AlO_x/SAM gate dielectrics with the same thickness and the same capacitance,[26,27,32] which further confirms that this effect occurs regardless of (although with a weak dependence on) the choice of the semiconductor. More importantly, Figure 2c shows that for each of the eight combinations of SAM and semiconductor, the threshold voltage is independent of the channel length down to 2 µm, confirming the absence of threshold-voltage roll-off in these TFTs, owing to the small thickness of the AlO_x/SAM gate dielectrics. For DNTT TFTs with the AlO_x/HC_{14}-PA SAM gate dielectric fabricated by electron-beam lithography, the absence of threshold-voltage roll-off has previously been confirmed for channel lengths down to 0.15 µm.[37]

Unlike the threshold voltage, which was found to be independent of the channel length, the effective carrier mobility

© 2014 WILEY-VCH Verlag GmbH & Co. KGaA, Weinheim

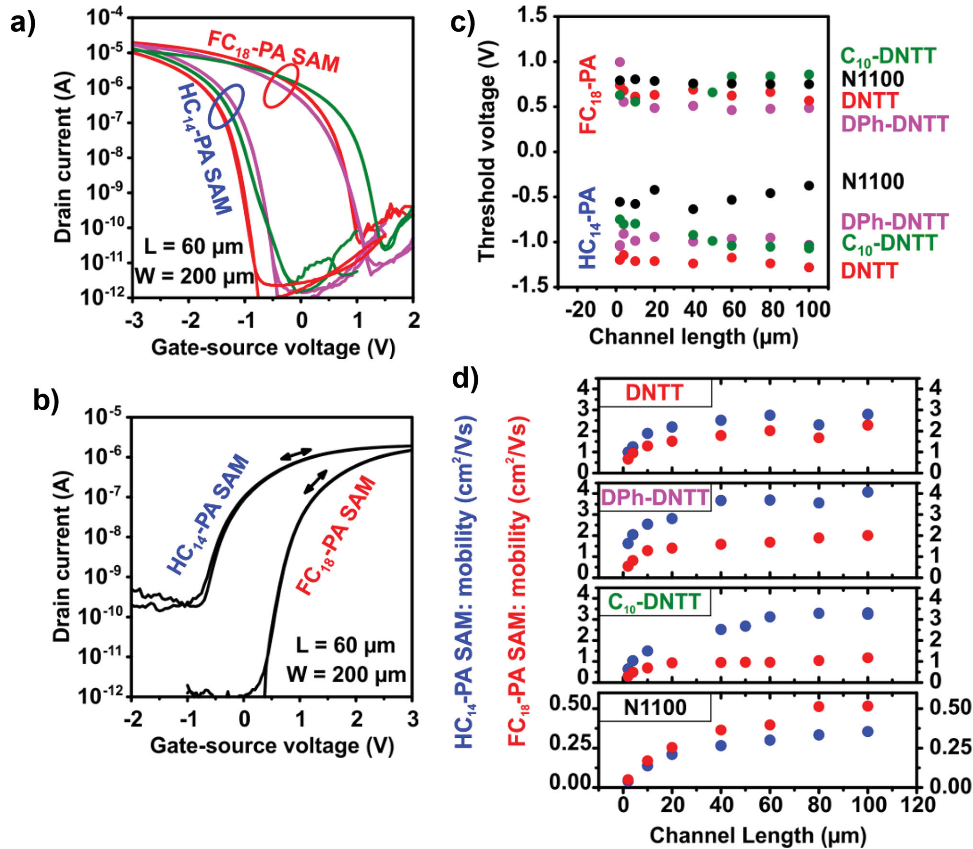

Figure 2. a,b) Transfer characteristics of flexible long-channel p-channel TFTs (red: DNTT; purple: DPh-DNTT; green: C_{10}-DNTT) and n-channel TFTs (N1100) with a gate dielectric composed of 3.6-nm-thick AlO_x and a self-assembled monolayer based on either an alkyl-phosphonic acid (HC_{14}-PA) or a fluoroalkyl-phosphonic acid (FC_{18}-PA). The measurements were performed with a drain-source voltage of –2.0 V for the p-channel TFTs and +1.5 V for the n-channel TFTs. c,d) Threshold voltages and effective mobilities of DNTT, DPh-DNTT, C_{10}-DNTT and N1100 TFTs with either of the two gate-dielectric SAMs as a function of the channel length.

decreases significantly when the channel length is reduced below about 20 µm. This is due to the fact that the channel resistance is proportional to the channel length, while the contact resistance is independent of the channel length, so that the relative influence of the contact resistance on the total device resistance increases when the channel length is reduced, causing the effective mobility to drop significantly below the intrinsic channel mobility at very small channel lengths,[6,7] and this can be seen in Figure 2d for each combination of SAM and semiconductor. Figure 2d also confirms that for all three p-channel semiconductors, the carrier mobilities are larger for the TFTs with the alkyl SAM than with the fluoroalkyl SAM, which is consistent with observations made previously for pentacene.[25–27]

Table 1. Effective field-effect mobility, subthreshold swing, intrinsic carrier mobility and width-normalized contact resistance of flexible DNTT, DPh-DNTT, C_{10}-DNTT and N1100 TFTs with either of the two different gate-dielectric SAMs (HC_{14}-PA or FC_{18}-PA). The width-normalized contact resistances were measured at a fixed overdrive voltage V_{GS}–V_{th} of –1.5 V (p-channel TFTs) and +1.5 V (n-channel TFTs).

Semiconductor	Carrier type	SAM for gate dielectric	Effective field-effect mobility (L = 60 µm)	Subthreshold swing (L = 60 µm)	Intrinsic carrier mobility (μ_0)	Width-normalized contact resistance ($R_C W$)
DNTT	p-channel TFT	HC_{14}-PA	2.7 cm²/Vs	100 mV/dec.	2.9 cm²/Vs	0.30 kΩ cm
		FC_{18}-PA	2.0 cm²/Vs	110 mV/dec.	2.2 cm²/Vs	0.69 kΩ cm
DPh-DNTT	p-channel TFT	HC_{14}-PA	3.7 cm²/Vs	100 mV /dec.	4.1cm²/Vs	0.16 kΩ cm
		FC_{18}-PA	1.6 cm²/Vs	160 mV/dec.	1.9 cm²/Vs	0.38 kΩ cm
C_{10}-DNTT	p-channel TFT	HC_{14}-PA	3.1 cm²/Vs	170 mV/dec.	3.6 cm²/Vs	0.47 kΩ cm
		FC_{18}-PA	0.9 cm²/Vs	140 mV/dec.	1.1 cm²/Vs	0.84 kΩ cm
N1100	n-channel TFT	HC_{14}-PA	0.3 cm²/Vs	180 mV/dec.	0.5 cm²/Vs	23 kΩ cm
		FC_{18}-PA	0.4 cm²/Vs	120 mV/dec.	0.8 cm²/Vs	15 kΩ cm

© 2014 WILEY-VCH Verlag GmbH & Co. KGaA, Weinheim

One explanation that has been suggested in literature is that the observed differences in carrier mobility are related to differences in the thin-film morphology of the organic semiconductor deposited onto the different dielectrics. For example, for pentacene TFTs with sol-gel-processed methacrylate siloxane gate dielectrics containing various amounts of a fluoroalkyl additive, Kwak et al. have seen a monotonic correlation between the surface energy of the dielectric (larger fluorine content leads to smaller surface energy), the grain size of the pentacene layer (smaller surface energy leads to smaller grain size), and the carrier mobility (smaller grain size leads to smaller carrier mobility).[38] A similar trend between the surface energy of the dielectric and the grain size of the pentacene layer (smaller surface energy leads to smaller grain size) was also seen by Yang et al.,[39] but Yang et al. measured larger carrier mobilities for smaller grain size (i.e., larger carrier mobilities for smaller surface energy).[39] The thin-film morphology of the four organic semiconductors investigated in our study and deposited onto substrates covered with either the alkyl SAM or the fluoroalkyl SAM are shown in Figure S1, Supporting Information (images obtained by atomic force microscopy, AFM) and Figure S2, Supporting Information (images obtained by scanning electron microscopy, SEM). Although the images reveal certain differences in the morphology depending on the type of SAM, it is difficult to draw meaningful conclusions regarding its impact on the carrier mobility, especially since the charge transport takes place in close proximity of the dielectric interface, a region that is not easily imaged by AFM or SEM. An alternative explanation for the observed differences in carrier mobility is the degree of energetic disorder induced in the semiconductor by the polar character of the SAM,[40–43] which may lead to charge trapping.[25,35,44]

In contrast to the p-channel semiconductors DNTT, DPh-DNTT and C_{10}-DNTT, in which the carrier mobilities are larger with the alkyl SAM than with the fluoroalkyl SAM, the opposite trend is seen for the n-channel semiconductor N1100, which shows larger mobilities with the fluoroalkyl SAM than with the alkyl SAM, due to the particular interactions between the fluoroalkyl substituents of the SAM and of the semiconductor that leads to a more favorable packing of the semiconductor molecules.[24]

Figure 2d further reveals that the ratio between the mobility obtained with the SAM that gives the greater mobility and that obtained with the SAM that gives the smaller mobility displays a dependence on the channel length that is unique for each of the four semiconductors. The fact that the relationship between the effective mobility and the channel length is so different for the various combinations of SAM and semiconductor indicates that the contact resistance of the TFTs depends heavily on both the semiconductor and the SAM. We have therefore employed the transmission line method (TLM)[5–7] to determine the contact resistance and the intrinsic channel mobility for each of the eight combinations of SAM and semiconductor. In order to account for the differences between the threshold voltages of the various TFTs, only data that were measured at a fixed gate overdrive voltage (i.e., at a fixed gate-source voltage above threshold; V_{GS}–V_{th}) were used for the TLM analysis; this assures that only contact resistances obtained at the same bias condition are compared. The TLM analysis is illustrated in **Figure 3**, and the results are summarized in Table 1 as well as in Table S2 and in Figure S3, Supporting Information.

The results of the TLM analysis in Figure 3 and Table 1 reveal that the magnitude of the influence of the choice of the SAM on the intrinsic carrier mobility is quite different for the various semiconductors. In particular, DNTT is much less sensitive to the choice of the SAM than DPh-DNTT and C_{10}-DNTT: the ratio between the intrinsic mobilities for the two SAMs is close to unity in the case of DNTT (2.9 cm^2/Vs on the alkyl SAM vs. 2.2 cm^2/Vs on the fluoroalkyl SAM), but greater than 3 in the case of C_{10}-DNTT (3.6 cm^2/Vs on the alkyl SAM vs. 1.1 cm^2/Vs on the fluoroalkyl SAM). As a result, DNTT is the semiconductor with the largest intrinsic mobility on the fluoroalkyl SAM (2.2 cm^2/Vs). This is somewhat surprising, because on the alkyl SAM, DNTT is easily outperformed by DPh-DNTT and C_{10}-DNTT, but it appears that on the fluoroalkyl SAM, the interactions of the fluoroalkyl substituents of the SAM with the phenyl or decyl substituents of DPh-DNTT or C_{10}-DNTT are unfavorable. The large intrinsic mobility of DNTT on the fluoroalkyl SAM implies a large effective mobility in long-channel TFTs, which is exactly what is seen in Figure 2d.

On the other hand, DPh-DNTT provides the smallest contact resistances on both SAMs (0.16 kΩ cm on the alkyl SAM, 0.38 kΩ cm on the fluoroalkyl SAM), and these small contact resistances are obviously a significant benefit in short-channel TFTs. Taking all of this into consideration, it becomes clear why on the fluoroalkyl SAM, DNTT outperforms DPh-DNTT and C_{10}-DNTT in long-channel TFTs, while DPh-DNTT emerges as the best choice for short-channels TFTs, regardless of the choice of the SAM.

The N1100 n-channel TFTs have a width-normalized contact resistance of 23 kΩ cm when using the alkyl SAM and 15 kΩ cm when using the fluoroalkyl SAM. The latter is the smallest contact resistance reported for organic n-channel TFTs fabricated on flexible substrates. (Smaller contact resistances have been reported for organic n-channel TFTs on rigid substrates[45] and for organic n-channel TFTs that cannot be operated in air.[46,47] However, compared with the contact resistances of the p-channel TFTs, which are below 1 kΩ cm for all three semiconductors, the contact resistances of the N1100 n-channel TFTs are larger by almost two orders of magnitude. Thus, the dynamic performance of complementary circuits, especially when based on TFTs with small channel lengths, will be limited by the n-channel TFTs, rather than by the p-channel TFTs, and since the contact resistance of the N1100 TFTs is smaller for the fluoroalkyl SAM than for the alkyl SAM (see Figure 3 and Table 1), it can be expected that complementary circuits fabricated using the fluoroalkyl SAM will provide better dynamic performance than complementary circuits fabricated using the alkyl SAM.

The perhaps somewhat surprising observation that the choice of the SAM has an impact not only on the intrinsic carrier mobility, but also on the contact resistance of the TFTs can be understood in the context of the current crowding model. In this model, the semiconductor regions underneath the source and drain contacts are considered as resistor networks, and the effective area available for the exchange of charge carriers between the contacts and the gate-induced carrier channel (and

© 2014 WILEY-VCH Verlag GmbH & Co. KGaA, Weinheim

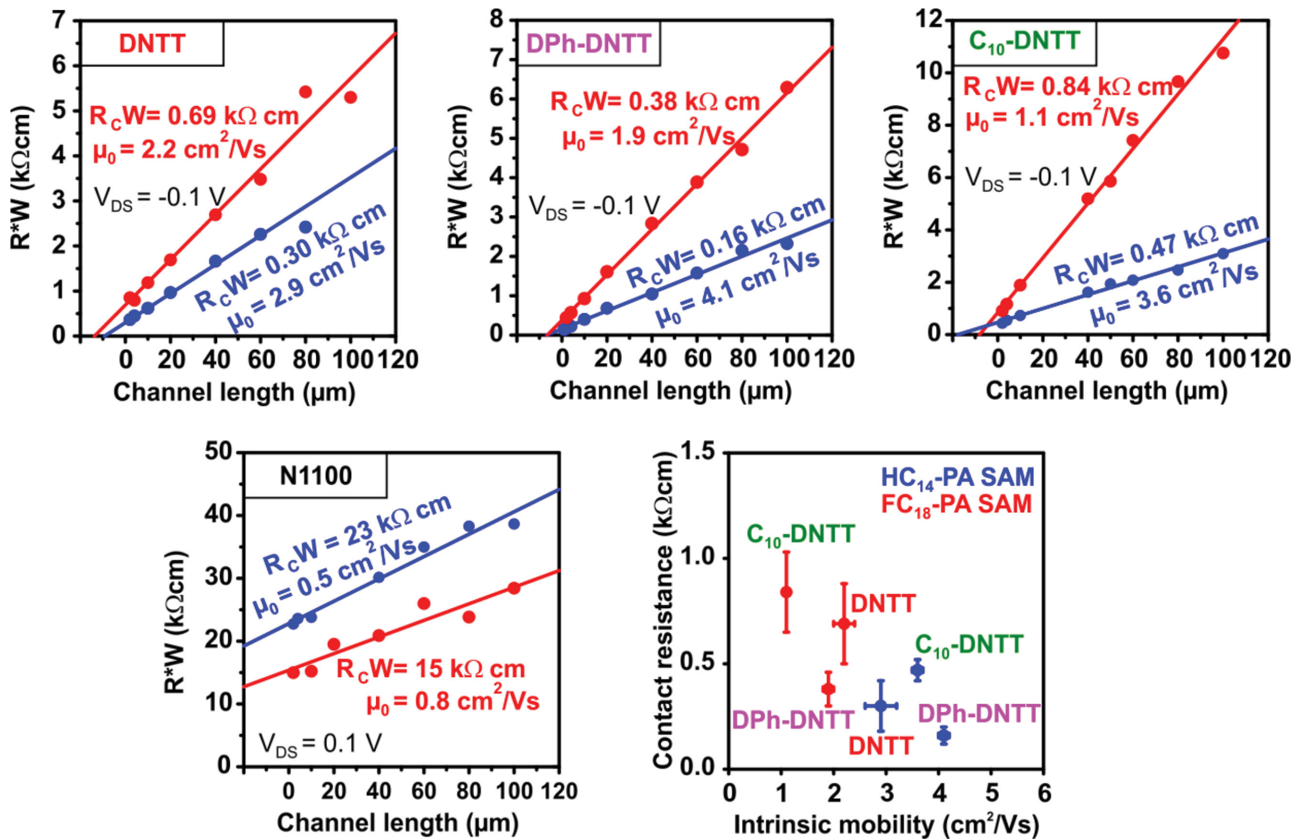

Figure 3. Transmission line method: channel-width-normalized total resistances of flexible DNTT, DPh-DNTT, C_{10}-DNTT p-channel and N1100 n-channel TFTs with either of the two gate-dielectric SAMs (HC_{14}-PA, blue; FC_{18}-PA, red) as a function of the channel length (2 to 100 μm). All resistances were measured at a fixed overdrive voltage V_{GS}–V_{th} of –1.5 V (p-channel TFTs) and +1.5 V (n-channel TFTs). Extrapolation to a channel length of zero yields the width-normalized contact resistance (R_CW); the inverse slope of the linear fit yields the intrinsic carrier mobility (μ_0). The error bars are based on the confidence intervals determined from the linear fits of the TLM measurements.

hence the contact resistance) is the result of a balance between the vertical contact resistances and the lateral channel sheet resistance,[45,48] both of which are to some extent affected by the intrinsic carrier mobility and hence by the choice of the SAM.

As mentioned above, the contact resistance is particularly dominant in TFTs that have a small channel length. **Figure 4** shows the measured transfer and output characteristics of flexible short-channel DPh-DNTT p-channel and N1100 n-channel TFTs fabricated using the fluoroalkyl-phosphonic acid (FC_{18}-PA) as part of the AlO_x/SAM gate dielectric. The TFTs have channel lengths of 10 μm, 1 μm and 0.5 μm. To our knowledge, there are only two previous reports of flexible organic TFTs with such a short channel length.[49,50] As can be seen in Figure 4, reducing the channel length from 10 μm to 0.5 μm produces virtually no degradation in the off-state drain current, the threshold voltage or the subthreshold slope of the TFTs. Even at a channel length of 0.5 μm, the on/off current ratio is still greater than 10^6 and the output curves still display reasonably good current saturation. The significant difference between the contact resistance of the DPh-DNTT p-channel TFTs (0.38 kΩ cm) and that of the N1100 n-channel TFTs (15 kΩ cm) is evident in the output characteristics, where the drain current at small drain-source voltages shows the desirable linear dependence on the drain-source voltage in the case of the DPh-DNTT TFTs, but is significantly suppressed in the case of the N1100 TFTs. The effective carrier mobilities extracted from the measured transfer characteristics of the short-channel TFTs are summarized in Table S3. The observation that these mobilities are notably smaller than the long-channel mobilities again illustrates the above-discussed relative influence of the contact resistance.

To evaluate the dynamic performance of the devices, we fabricated 11-stage complementary ring oscillators on flexible PEN substrates (see Figure S4) using Polyera ActivInk N1100 as the semiconductor for the n-channel TFTs and either DNTT or DPh-DNTT as the semiconductor for the p-channel TFTs, and using either the alkyl-phosphonic acid (HC_{14}-PA) or the fluoroalkyl-phosphonic acid (FC_{18}-PA) as part of the AlO_x/SAM gate dielectric. The results are summarized in **Figure 5** and Table S4, Supporting Information. The first observation is that these circuits can be operated with supply voltages as low as 1 V, owing to the small thickness and large capacitance of the AlO_x/SAM gate dielectrics. The second observation is that smaller channel lengths result in faster circuit operation, as expected based on the fact that the gate capacitance scales linearly with the lateral TFT dimensions.[7] The third observation is that the measured signal propagation delays are shorter when the fluoroalkyl SAM, rather than the alkyl SAM, is employed

© 2014 WILEY-VCH Verlag GmbH & Co. KGaA, Weinheim

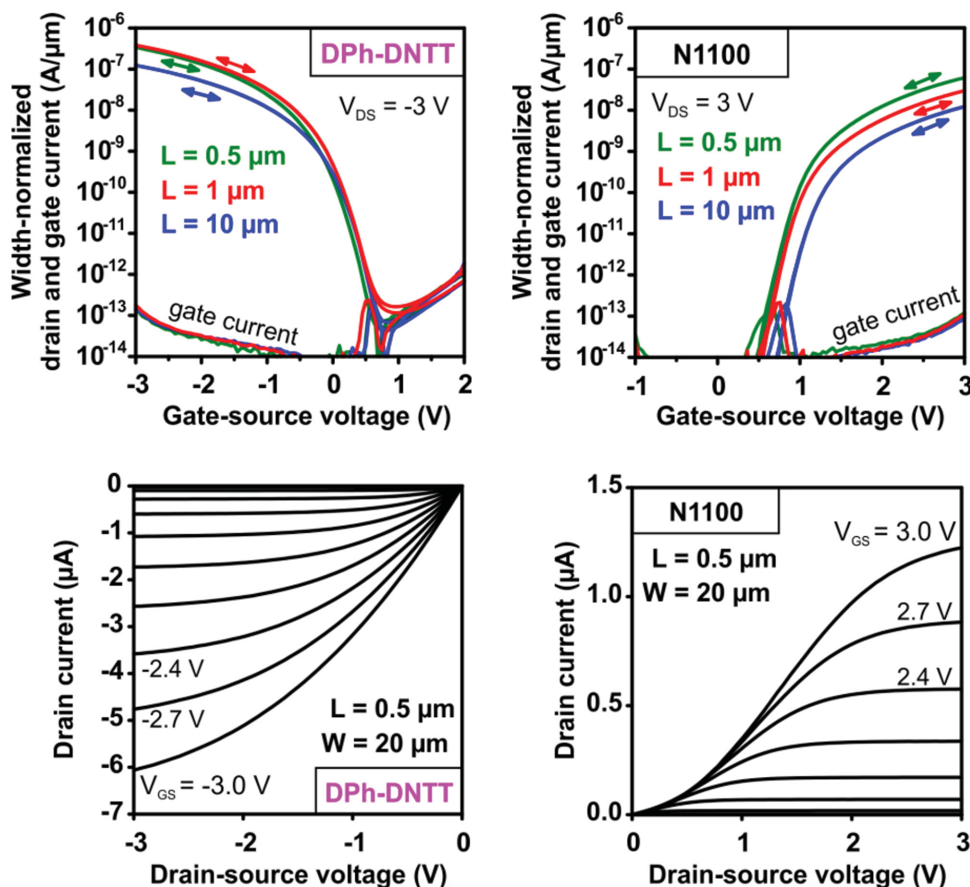

Figure 4. Transfer and output characteristics of flexible short-channel DPh-DNTT p-channel and N1100 n-channel TFTs with AlO_x/FC_{18}-PA SAM gate dielectrics on flexible PEN substrates. The TFTs have the following channel lengths and channel widths: L = 0.5 µm, W = 20 µm; L = 1 µm, W = 100 µm; L = 10 µm, W = 100 µm.

(provided all other parameters are the same). This is consistent with the above-discussed observations that the contact resistance of the N1100 n-channel TFTs is larger than the contact resistances of the p-channel TFTs (so that the dynamic performance of complementary circuits is limited by the n-channel TFTs, especially when the channel lengths are very small) and that the contact resistance of the N1100 TFTs is smaller for the fluoroalkyl SAM than for the alkyl SAM (see Figure 3 and Table 1). The fourth observation is that the measured signal propagation delays are shorter when the N1100 n-channel TFTs

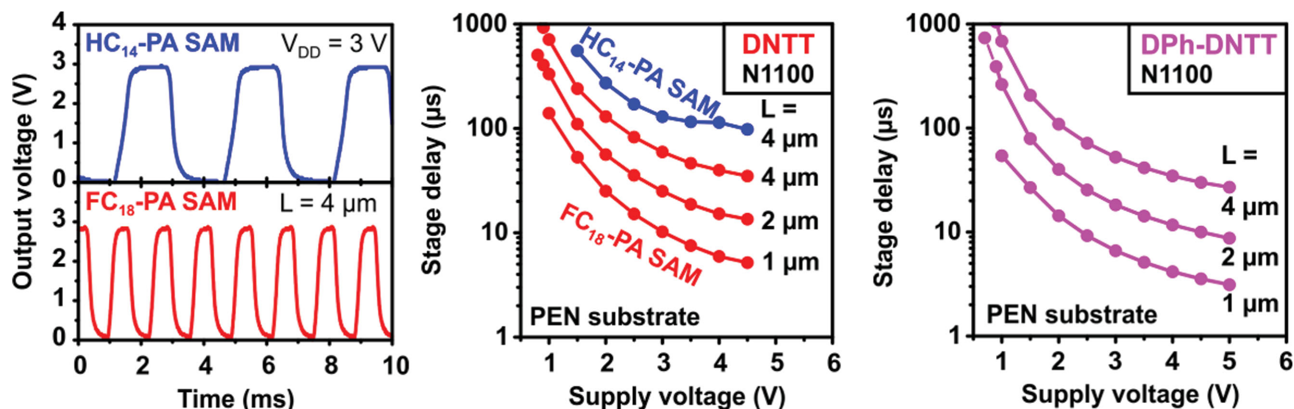

Figure 5. Output signals (both at a supply voltage V_{DD} of 3 V) and signal propagation delays (plotted as a function of the supply voltage) of 11-stage complementary ring oscillators fabricated on flexible PEN substrates using N1100 as the semiconductor for the n-channel TFTs, either DNTT or DPh-DNTT as the semiconductor for the p-channel TFTs and either of the two gate-dielectric SAMs (HC_{14}-PA and FC_{18}-PA). The TFTs have a channel length of either 4 µm, 2 µm or 1 µm. The circuits operate with supply voltages as low as 1 V and with signal propagation delays as short as 3.1 µs per stage.

© 2014 WILEY-VCH Verlag GmbH & Co. KGaA, Weinheim

are complemented by p-channel TFTs based on DPh-DNTT, rather than DNTT. This is consistent with the above-discussed observation that DPh-DNTT provides the smallest contact resistance of all semiconductors (0.38 kΩ cm on the fluoroalkyl SAM; see Figure 3 and Table 1). The shortest signal propagation delay per stage is 3.1 μs, measured on a ring oscillator based on DPh-DNTT p-channel and N1100 n-channel TFTs with the AlO_x/FC_{18}-PA SAM gate dielectric, having a channel length of 1 μm and being operated with a supply voltage of 5 V. This signal propagation delay is similar to or better than the shortest signal delays reported for flexible organic complementary ring oscillators.[45,51–55]

In summary, we have fabricated low-voltage p-channel and n-channel organic thin-film transistors on flexible plastic substrates with channel lengths as short as 0.5 μm using either DNTT, DPh-DNTT, C_{10}-DNTT or Polyera ActivInk N1100 as the semiconductor and either an alkyl-phosphonic acid or a fluoroalkyl-phosphonic acid self-assembled monolayer for the ultra-thin gate dielectric. Long-channel transistors have effective field-effect mobilities ranging from 0.5 cm^2/Vs for the n-channel TFTs to 4.2 cm^2/Vs for the p-channel TFTs. For each of the eight combinations of semiconductor (DNTT, DPh-DNTT, C_{10}-DNTT, N1100) and SAM (HC_{14}-PA, FC_{18}-PA) we have determined the transistor's contact resistances and intrinsic carrier mobilities using the transmission line method for devices with channel lengths ranging from 100 μm to 2 μm. In the p-channel TFTs, these three parameters (effective mobility, intrinsic mobility, contact resistance) are favored by the use of the alkyl SAM, whereas in the n-channel TFTs they benefit from the use of the fluoroalkyl SAM. Since it is difficult to pattern two different SAMs with high resolution on the same substrate, we have analyzed which compromise in terms of choosing the same SAM for both types of transistors will give the better dynamic performance in complementary circuits based on p-channel and n-channel TFTs with very small channel lengths. Of the three p-channel semiconductors, DPh-DNTT was found to provide the smallest contact resistance (0.38 kΩ cm on the fluoroalkyl SAM), and therefore the shortest signal propagation delays (as short as 3.1 μs per stage, measured in flexible 11-stage ring oscillators based on TFTs with a channel length of 1 μm) when combined with N1100 as the semiconductor for the n-channel TFTs and using the fluoroalkyl SAM for the gate dielectric. These results illustrate the critical role of the gate dielectric in determining the performance of organic transistors and circuits.

Experimental Section

DNTT, C_{10}-DNTT and DPh-DNTT were synthesized as reported earlier.[1–3] ActivInk N1100 was purchased from Polyera, Skokie, IL, USA. Tetradecylphosphonic acid was purchased from PCI Synthesis, Newburyport, MA, USA. 12,12,13,13,14,14,15,15,16,16,17,17,18,18,18-pentadecafluoro-octadecylphosphonic acid was synthesized and kindly provided by Matthias Schlörholz.[32] 125-μm-thick flexible polyethylene naphthalate film (Teonex Q65 PEN) was kindly provided by William A. MacDonald, DuPont Teijin Films, Wilton, UK.

All TFTs and ring oscillators were fabricated on flexible PEN substrates. Aluminum gate electrodes with a thickness of 30 nm were deposited onto the PEN substrates by thermal evaporation in vacuum. The gate dielectric is composed of an oxygen-plasma-grown AlO_x layer with thickness of 3.6 nm and a solution-processed self-assembled monolayer (SAM)[56] of either tetradecylphosphonic acid (HC_{14}-PA) or 12,12,13,13,14,14,15,15,16,16,17,17,18,18,18-pentadecafluoro-octadecylphosphonic acid (FC_{18}-PA). The SAMs have a thickness of 1.7 or 2.1 nm, and their quality was confirmed by static contact angle measurements.[26,32] The AlO_x/SAM gate dielectrics have a capacitance per unit area of 0.7 or 0.6 μF/cm^2. Organic semiconductor films with a thickness of 20 or 25 nm were deposited onto the AlO_x/SAM gate dielectrics by sublimation in vacuum. During the semiconductor deposition, the substrate was held at a temperature of 60 °C (DNTT), 80 °C (DPh-DNTT, C_{10}-DNTT) or 140 °C (N1100). TFTs were completed by the vacuum deposition of gold source and drain contacts. The metal and semiconductor layers were patterned using high-resolution silicon stencil masks.[7,9,11] All measurements were performed in ambient air at room temperature.

Supporting Information

Supporting Information is available from the Wiley Online Library or from the author.

Acknowledgments

This work was partially funded by BASF SE, by the German Ministry of Education and Research (BMBF) under Grants 13N10763 (KOSADIS; Research Network Forum Organic Electronics) and 1612000463 (KoSiF) and by the German Research Foundation (DFG) under Grants KL 2223/5-1 and KL 2223/5-2.

Received: July 31, 2014
Revised: September 10, 2014
Published online: October 20, 2014

[1] T. Yamamoto, K. Takimiya, *J. Am. Chem. Soc.* **2007**, *129*, 2224.

[2] M. J. Kang, I. Doi, H. Mori, E. Miyazaki, K. Takimiya, M. Ikeda, H. Kuwabara, *Adv. Mater.* **2011**, *23*, 122.

[3] M. J. Kang, E. Miyazaki, I. Osaka, K. Takimiya, A. Nakao, *ACS Appl. Mater. Interfaces* **2013**, *5*, 2331.

[4] K. Niimi, M. J. Kang, E. Miyazaki, I. Osaka, K. Takimiya, *Org. Lett.* **2011**, *13*, 3430.

[5] R. Hofmockel, U. Zschieschang, U. Kraft, R. Rödel, N. H. Hansen, M. Stolte, F. Würthner, K. Takimiya, K. Kern, J. Pflaum, H. Klauk, *Org. Electronics* **2013**, *14*, 3213.

[6] T. Matsumoto, W. Ou-Yang, K. Miyake, T. Uemura, J. Takeya, *Org. Electronics* **2013**, *14*, 2590.

[7] F. Ante, D. Kälblein, T. Zaki, U. Zschieschang, K. Takimiya, M. Ikeda, T. Sekitani, T. Someya, J. N. Burghartz, K. Kern, H. Klauk, *Small* **2012**, *8*, 73.

[8] E. D. Głowacki, M. Irimia-Vladu, M. Kaltenbrunner, J. Gasiorowski, M. S. White, U. Monkowius, G. Romanazzi, G. P. Suranna, P. Mastrorilli, T. Sekitani, S. Bauer, T. Someya, L. Torsi, N. S. Sariciftci, *Adv. Mater.* **2013**, *25*, 1563.

[9] T. Zaki, F. Ante, U. Zschieschang, J. Butschke, F. Letzkus, H. Richter, H. Klauk, J. N. Burghartz, *IEEE J. Solid-State Circ.* **2012**, *47*, 292.

[10] U. Zschieschang, M. J. Kang, K. Takimiya, T. Sekitani, T. Someya, T. W. Canzler, A. Werner, J. Blochwitz-Nimoth, H. Klauk, *J. Mater. Chem.* **2012**, *22*, 4273.

[11] U. Zschieschang, R. Hofmockel, R. Rödel, U. Kraft, M. J. Kang, K. Takimiya, T. Zaki, F. Letzkus, J. Butschke, H. Richter, J. N. Burghartz, H. Klauk, *Org. Electronics* **2013**, *14*, 1516.

© 2014 WILEY-VCH Verlag GmbH & Co. KGaA, Weinheim

[12] T. Yokota, K. Kuribara, T. Tokuhara, U. Zschieschang, H. Klauk, K. Takimiya, Y. Sadamitsu, M. Hamada, T. Sekitani, T. Someya, *Adv. Mater.* **2013**, *25*, 3639.
[13] B. Peng, P. K. L. Chan, *Org. Electronics* **2014**, *15*, 203.
[14] U. Zschieschang, T. Yamamoto, K. Takimiya, H. Kuwabara, M. Ikeda, T. Sekitani, T. Someya, H. Klauk, *Adv. Mater.* **2011**, *23*, 654.
[15] Y. Kubota, T. Matsumoto, H. Tsuji, N. Suzuki, S. Imai, H. Kobayashi, *IEEE Trans. Electr. Dev.* **2012**, *59*, 385.
[16] G. H. Gelinck, H. E. A. Huitema, E. van Veenendaal, E. Cantatore, L. Schrijnemakers, J. B. P. H. van der Putten, T. C. T. Geuns, M. Beenhakkers, J. B. Giesbers, B. H. Huisman, E. J. Meijer, E. M. Benito, F. J. Touwslager, A. W. Marsman, B. J. E. van Rens, D. M. de Leeuw, *Nat. Mater.* **2004**, *3*, 106.
[17] D. Raiteri, P. van Lieshout, A. van Roermund, E. Cantatore, *IEEE J. Solid-State Circ.* **2014**, *49*, 524.
[18] D. Bode, C. Rolin, S. Schols, M. Debucquoy, S. Steudel, G. H. Gelinck, J. Genoe, P. Heremans, *IEEE Trans. Electr. Dev.* **2010**, *57*, 201.
[19] T. N. Ng, D. E. Schwartz, L. L. Lavery, G. L. Whiting, B. Russo, B. Krusor, J. Veres, P. Bröms, L. Herlogsson, N. Alam, O. Hagel, J. Nilsson, C. Karlsson, *Sci. Rep.* **2012**, *2*, 585.
[20] C. Wang, H. Dong, W. Hu, Y. Liu, D. Zhu, *Chem. Rev.* **2012**, *112*, 2208.
[21] B. A. Jones, M. J. Ahrens, M. H. Yoon, A. Facchetti, T. J. Marks, M. R. Wasielewski, *Angew. Chem. Int. Ed.* **2004**, *43*, 6363.
[22] B. A. Jones, A. Facchetti, M. R. Wasielewski, T. J. Marks, *J. Am. Chem. Soc.* **2007**, *129*, 15259.
[23] J. Soeda T. Uemura, Y. Mizuno, A. Nakao, Y. Nakazawa, A. Facchetti, J. Takeya, *Adv. Mater.* **2011**, *23*, 3681.
[24] M. Sejfić, U. Kraft, N. H. Hansen, J. Pflaum, U. Zschieschang, H. Klauk, R. T. Weitz, *International Symposium on Flexible Organic Electronics,*Thessaloniki, Greece, **2013.**
[25] K. P. Pernstich, S. Haas, D. Oberhoff, C. Goldmann, D. J. Gundlach, B. Batlogg, A. N. Rashid, G. Schitter, *J. Appl. Phys.* **2004**, *96*, 6431.
[26] U. Kraft, U. Zschieschang, F. Ante, D. Kälblein, C. Kamella, K. Amsharov, M. Jansen, K. Kern, E. Weber, H. Klauk, *J. Mater. Chem.* **2010**, *20*, 6416.
[27] M. Salinas, C. M. Jäger, A. Y. Amin, P. O. Dral, T. Meyer-Friedrichsen, A. Hirsch, T. Clark, M. Halik, *J. Am. Chem. Soc.* **2012**, *134*, 12648.
[28] J. W. Ward, M. A. Loth, R. J. Kline, M. Coll, C. Ocal, J. E. Anthony, O. D. Jurchescu, *J. Mater. Chem.* **2012**, *22*, 19047
[29] J. W. Ward, R. Li, A. Obaid, M. M. Payne, D.-M. Smilgies, J. E. Anthony, A. Amassian, O. D. Jurchescu, *Adv. Funct. Mater.* **2014**, *24*, 5052.
[30] I. Hirata, U. Zschieschang, F. Ante, T. Yokota, K. Kuribara, T. Yamamoto, K. Takimiya, M. Ikeda, H. Kuwabara, H. Klauk, T. Sekitani, T. Someya, *MRS Commun.* **2011**, *1*, 33.
[31] S. Kobayashi, T. Nishikawa, T. Takenobu, S. Mori, T. Shimoda, T. Mitani, H. Shimotani, N. Yoshimoto, S. Ogawa, Y. Iwasa, *Nat. Mater.* **2004**, *3*, 317.
[32] U. Zschieschang, F. Ante, M. Schlörholz, M. Schmidt, K. Kern, H. Klauk, *Adv. Mater.* **2010**, *22*, 4489.
[33] C. Huang, H. E. Katz, J. E. West, *Langmuir* **2007**, *23*, 13223.
[34] S. K. Possanner, K. Zojer, P. Pacher, E. Zojer, F. SchÃürrer, *Adv. Funct. Mater.* **2009**, *19*, 958.
[35] F. Gholamrezaie, A. M. Andringa, W. S. Roelofs, A. Neuhold, M. Kemerink, P. W. M. Blom, D. M. de Leeuw, *Small* **2012**, *8*, 241.
[36] A. Valletta, P. Gaucci, L. Mariucci, A. Pecora, M. Cuscuna, L. Maiolo, G. Fortunato, S. D. Brotherton, *Appl. Phys. Lett.* **2009**, *95*, 033507.
[37] F. Ante, D. Kälblein, U. Zschieschang, T. W. Canzler, A. Werner, K. Takimiya, M. Ikeda, T. Sekitani, T. Someya, H. Klauk, *Small* **2011**, *7*, 1186.
[38] S.-Y. Kwak, C. G. Choi, B.-S. Bae, *Electrochem. Solid-State Lett.* **2009**, *12*, G37.
[39] S. Y. Yang, K. Shin, C. E. Park, *Adv. Funct. Mater.* **2005**, *15*, 18006.
[40] J. Veres, S. D. Ogier, S. W. Leeming, D. C. Cupertino, S. M. Khaffaf, *Adv. Funct. Mater.* **2003**, *13*, 199.
[41] A. F. Stassen, R. W. I. de Boer, N. N. Iosad, A. F. Morpurgo, *Appl. Phys. Lett.* **2004**, *85*, 3899.
[42] N. G. Martinelli, M. Savini, L. Muccioli, Y. Olivier, F. Castet, C. Zannoni, D. Beljonne, J. Cornil, *Adv. Funct. Mater.* **2009**, *19*, 3254.
[43] A. Mityashin, O. M. Roscioni, L. Muccioli, C. Zannoni, V. Geskin, J. Cornil, D. Jansse, S. Steudel, J. Genoe, P. Heremans, *ACS Appl. Mater. Interfaces* **2014**, *6*, 15372.
[44] S. Scheinert, K. P. Pernstich, B. Batlogg, G. Paasch, *J. Appl. Phys.* **2007**, *102*, 104503.
[45] R. Rödel, F. Letzkus, T. Zaki, J. N. Burghartz, U. Kraft, U. Zschieschang, K. Kern, H. Klauk, *Appl. Phys. Lett.* **2013**, *102*, 233303.
[46] M. Kitamura, S. Aomori, J. H. Na, Y. Arakawa, *Appl. Phys. Lett.* **2008**, *93*, 033313.
[47] N.-K. Kim, D. Khim, Y. Xu, S.-H. Lee, M. Kang, J. Kim, A. Facchetti, Y.-Y. Noh, D.-Y. Kim, *ACS Appl. Mater. Interfaces* **2014**, *6*, 9614.
[48] D. Schroder, *Semiconductor Materials and Device Characterization* Wiley, Hoboken, NJ, USA **2008**.
[49] P. F. Moonen, B. Vratzov, W. T. T. Smaal, B. K. C. Kjellander, G. H. Gelinck, E. R. Meinders, J. Huskens, *Org. Electronics* **2012**, *13*, 3004.
[50] F. Zanella, N. Marjanovic, R. Ferrini, H. Gold, A. Haase, A. Fian, B. Stadlober, R. Müller, J. Genoe, H. Hirshy, A. Drost, M. König, K. D. Lee, J. Ring, R. Pretot, C. C. Enz, J. M. Sallese, *Org. Electronics* **2013**, *14*, 2756.
[51] W. Smaal, C. Kjellander, Y. Jeong, A. Tripathi, B. van der Putten, A. Facchetti, H. Yan, J. Quinn, J. Anthony, K. Myny, W. Dehaen, G. Gelinck, *Org. Electronics* **2012**, *13*, 1686.
[52] K. J. Baeg, S.-W. Jung, D. Khim, J. Kim, D.-Y. Kim, J. B. Koo, J. R. Quinn, A. Facchetti, I.-K. You,Y.-Y. Noh , *Org. Electronics* **2013**, *14*, 1407.
[53] T. H. Ke, R. Müller, B. Kama, M. Rockele, A. Chasin, K. Myny, S. Steudel, W. D. Oosterbaan, L. Lutsen, J. Genoe, L. van Leuken, B. van der Putten, P. Heremans, *Org. Electronics* **2014**, *15*, 1229
[54] D. Raiteri, P. van Lieshout, A. van Roermund, E. Cantatore, *IEEE J. Solid-State Circuits* **2014**, *49*, 524.
[55] M. Benwadih, A. Aliane, S. Jacob, J. Bablet, R. Coppard, I. Chartier, *Org. Electronics* **2014**, *15*, 614.
[56] H. Klauk, U. Zschieschang, J. Pflaum, M. Halik, *Nature* **2007**, *445*, 745.

© 2014 WILEY-VCH Verlag GmbH & Co. KGaA, Weinheim

Copyright WILEY-VCH Verlag GmbH & Co. KGaA, 69469 Weinheim, Germany, 2013.

Supporting Information

Flexible Low-Voltage Organic Complementary Circuits: Finding the Optimum Combination of Semiconductors and Monolayer Gate Dielectrics

Ulrike Kraft, Mirsada Sejfić, Myeong Jin Kang, Kazuo Takimiya, Tarek Zaki, Harald Richter, Florian Letzkus, Joachim N. Burghartz, Edwin Weber, and Hagen Klauk*

Table S1. Effective field-effect mobilities and subthreshold swings of flexible DNTT, DPh-DNTT, C_{10}-DNTT and N1100 TFTs with a channel length of 60 µm and with either of the two different gate-dielectric SAMs (HC_{14}-PA or FC_{18}-PA). The values were extracted from the transfer characteristics in **Figure 2**. The observation that the subthreshold swing is greater (by a factor of 1.7 to 3) than the room-temperature limit of 58 mV/decade is related to the density of trap states at the semiconductor/dielectric interface, which is affected by several parameters, including the surface roughness of the plastic substrate.

semiconductor	**carrier type**	**SAM for gate dielectric**	**effective field-effect mobility**	**subthreshold swing**
DNTT	p-channel TFT	HC_{14}-PA	2.7 cm^2/Vs	100 mV/decade
		FC_{18}-PA	2.0 cm^2/Vs	110 mV /decade
DPh-DNTT	p-channel TFT	HC_{14}-PA	3.7 cm^2/Vs	100 mV /decade
		FC_{18}-PA	1.6 cm^2/Vs	160 mV /decade
C_{10}-DNTT	p-channel TFT	HC_{14}-PA	3.1 cm^2/Vs	170 mV /decade
		FC_{18}-PA	0.9 cm^2/Vs	140 mV /decade
N1100	n-channel TFT	HC_{14}-PA	0.3 cm^2/Vs	180 mV /decade
		FC_{18}-PA	0.4 cm^2/Vs	120 mV /decade

Table S2. Width-normalized contact resistances and intrinsic carrier mobilities of flexible DNTT, DPh-DNTT, C10-DNTT and N1100 TFTs with either of the two different gate-dielectric SAMs (HC14-PA or FC18-PA). The values were extracted from the TLM analysis shown in Figure 3.
p-channel TFTs: V_{GS}-V_{th} = -1.5 V; V_{DS} = -0.1 V
n-channel TFTs: V_{GS}-V_{th} = +1.5 V; V_{DS} = +0.1 V

semiconductor	**carrier type**	**SAM for gate dielectric**	**intrinsic carrier mobility (μ_0)**	**width-normalized contact resistance (R_CW)**	**coefficient of determination (R^2) of the linear fit**
DNTT	p-channel TFT	HC_{14}-PA	2.9 ± 0.3 cm^2/Vs	0.30 ± 0.12 kΩcm	0.970
		FC_{18}-PA	2.2 ± 0.2 cm^2/Vs	0.69 ± 0.19 kΩcm	0.971
DPh-DNTT	p-channel TFT	HC_{14}-PA	4.1 ± 0.1 cm^2/Vs	0.16 ± 0.04 kΩcm	0.992
		FC_{18}-PA	1.9 ± 0.1 cm^2/Vs	0.38 ± 0.08 kΩcm	0.996
C_{10}-DNTT	p-channel TFT	HC_{14}-PA	3.6 ± 0.1 cm^2/Vs	0.47 ± 0.05 kΩcm	0.992
		FC_{18}-PA	1.1 ± 0.04 cm^2/Vs	0.84 ± 0.19 kΩcm	0.993
N1100	n-channel TFT	HC_{14}-PA	0.5 ± 0.04 cm^2/Vs	23 ± 1 kΩcm	0.972
		FC_{18}-PA	0.8 ± 0.1 cm^2/Vs	15 ± 1 kΩcm	0.896

Table S3. Effective field-effect mobilities of flexible short-channel DPh-DNTT p-channel and N1100 n-channel TFTs for three different channel lengths. The values were extracted from the transfer characteristics shown in **Figure 4**.

semiconductor	carrier type	SAM for gate dielectric	effective field-effect mobility (μ_{eff})		
			L = 0.5 µm W = 20 µm	L = 1 µm W = 100 µm	L = 10 µm W = 100 µm
DNTT	p-channel TFT	FC_{18}-PA	n/a	0.08 cm^2/Vs	0.40 cm^2/Vs
DPh-DNTT	p-channel TFT	FC_{18}-PA	0.08 cm^2/Vs	0.16 cm^2/Vs	0.51 cm^2/Vs
N1100	n-channel TFT	FC_{18}-PA	0.04 cm^2/Vs	0.04 cm^2/Vs	0.14 cm^2/Vs

Table S4. Signal propagation delays measured in flexible 11-stage complementary ring oscillators based on DNTT or DPh-DNTT p-channel and N1100 n-channel TFTs with either of the two different gate-dielectric SAMs (HC_{14}-PA or FC_{18}-PA) and various channel lengths (4 µm, 2 µm or 1 µm), operated at a supply voltage of 4 V. The values were extracted from the measurements shown in **Figure 5**.

semiconductor for p-channel TFTs	semiconductor for n-channel TFTs	SAM for gate dielectric	signal propagation delay at 4V		
			L = 4 µm L_C = 20 µm	L = 2 µm L_C = 10 µm	L = 1 µm L_C = 5 µm
DNTT	N1100	HC_{14}-PA	114 µs	n/a	n/a
DNTT	N1100	FC_{18}-PA	40 µs	15 µs	6.0 µs
DPh-DNTT	N1100	FC_{18}-PA	35 µs	12 µs	4.2 µs

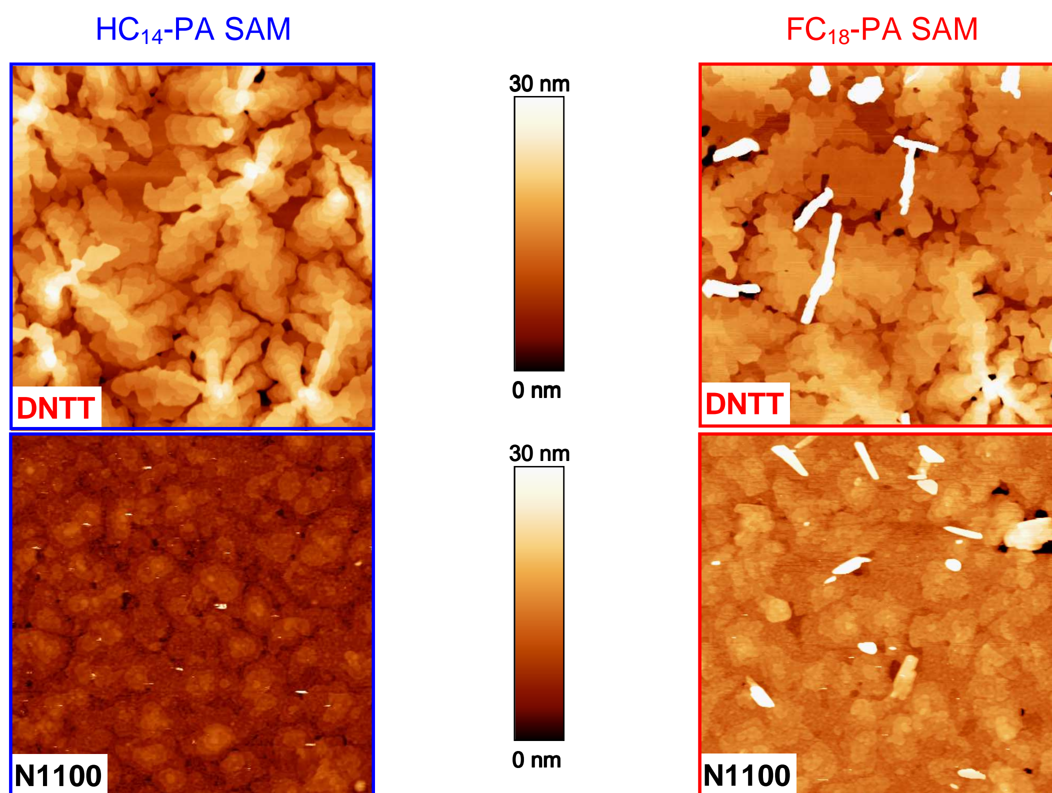

Figure S1. Morphology of thin-films of the organic semiconductors deposited onto either AlO_x/HC_{14}-PA SAM or AlO_x/FC_{18}-PA SAM gate dielectrics. The images were obtained by atomic force microscopy (AFM) in tapping mode. The image size is 5 µm × 5 µm.

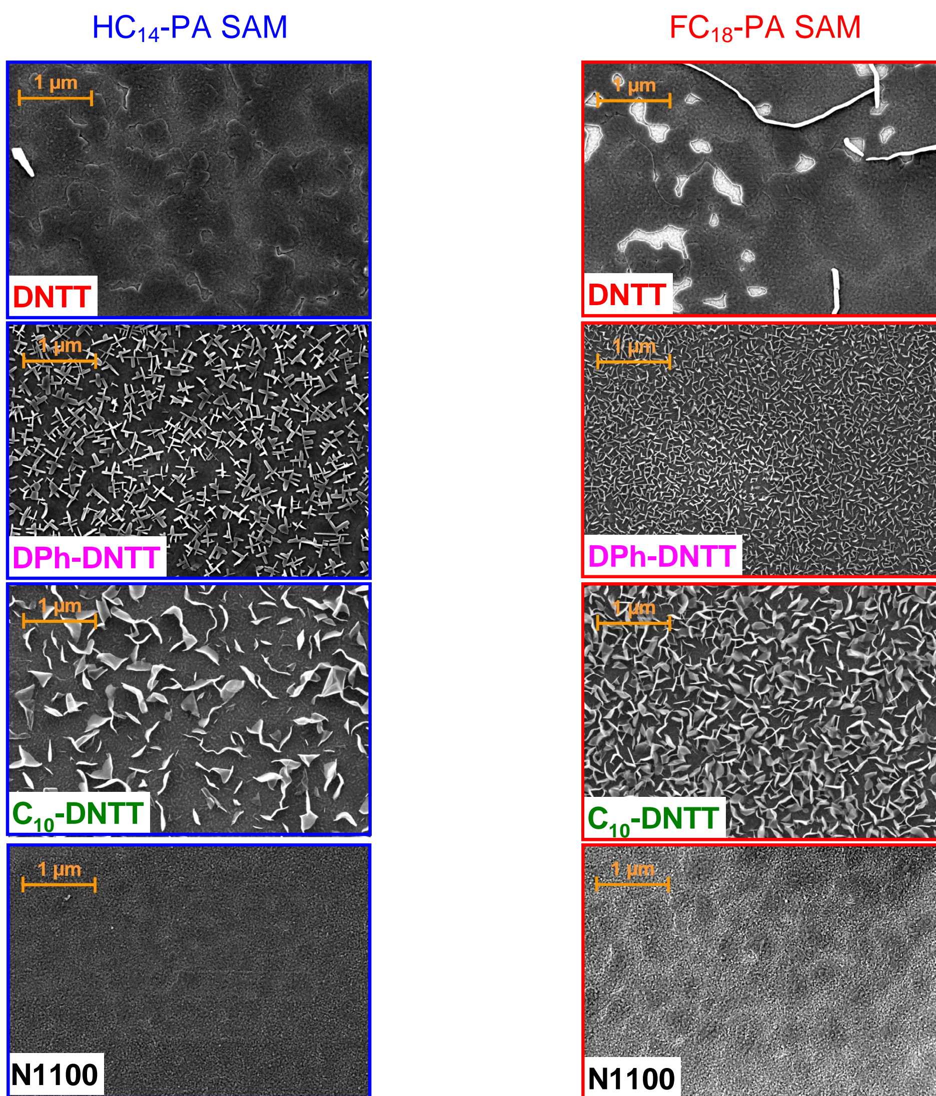

Figure S2. Morphology of thin-films of the organic semiconductors deposited onto either AlO_x/HC_{14}-PA SAM or AlO_x/FC_{18}-Pa SAM gate dielectrics. The images were obtained by scanning electron microscopy (SEM) with an acceleration voltage of 1.5 kV. The images have a width of 5 µm.

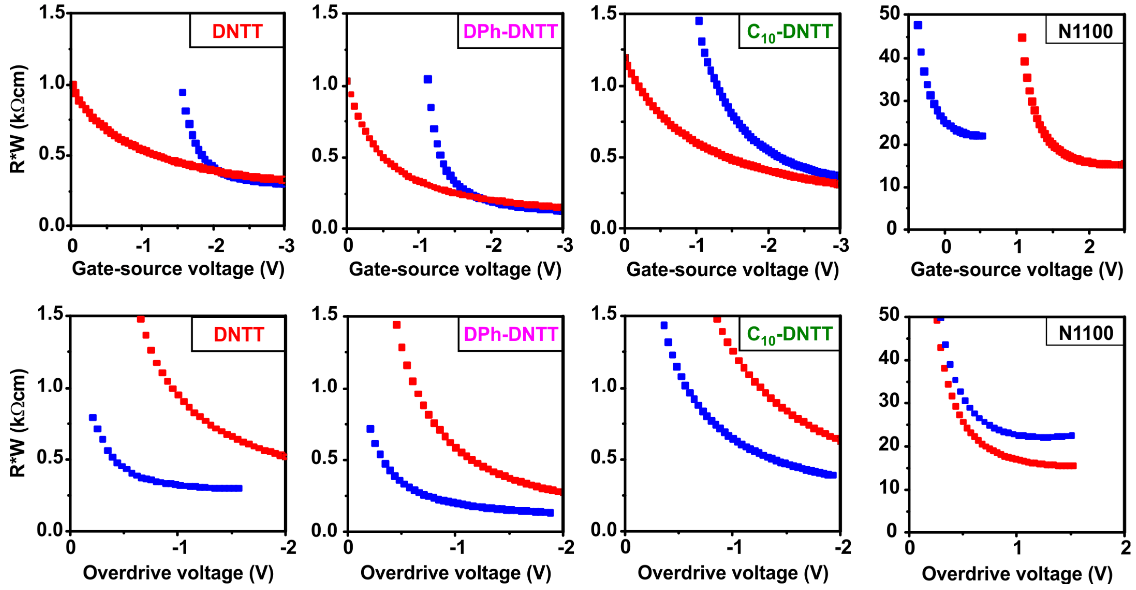

Figure S3. Channel-width-normalized contact resistance of flexible DNTT, DPh-DNTT, C_{10}-DNTT p-channel TFTs and N1100 n-channel TFTs with either of the two different gate-dielectric SAMs (HC_{14}-PA, blue; FC_{18}-PA, red) plotted once as a function of the applied gate-source voltage (V_{GS}) and once as a function of the gate overdrive voltage (V_{GS}-V_{th}). The values were extracted from the TLM analysis shown in Figure 3 at a drain-source voltage of -0.1 V (p-channel TFTs) or +0.1 V (n-channel TFTs). As can be seen, the contact resistance decreases with increasing gate-source or overdrive voltage. This is in agreement with the current crowding model [ref. S1, 45, 48] and can be explained with the fact that a larger gate-source voltage induces a greater charge-carrier density at the semiconductor/dielectric interface, which leads to a smaller sheet resistance, hence to a smaller horizontal component of the contact resistance, and thus to a larger area available for charge exchange between the contacts and the semiconductor [S2].

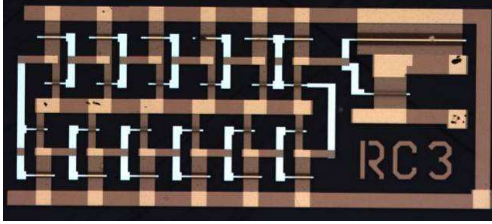

Figure S4. Photograph of an 11-stage complementary ring oscillator based on organic p-channel and n-channel TFTs with a channel length of 1 µm fabricated on a flexible plastic substrate.

Influence of the reduction of the channel length on the dynamic performance

When the channel length of a field-effect transistor is reduced, the effective carrier mobility decreases (see Figure 2). The reason is that the channel resistance is proportional to the channel length ($R_{channel} \sim L$), while the contact resistance is independent of the channel length, so that the relative influence of the contact resistance on the total device resistance increases when the channel length is reduced ($R_{total} = R_{channel} + R_{contact}$).

However, the cutoff frequency (f_T), *i.e.*, the dynamic performance of the transistor, is affected not only by the carrier mobility, but also by the gate capacitance ($f_T \sim 1/C_{gate}$) and thus by the lateral transistor dimensions [37]:

$$f_T \sim \frac{g_m}{2\pi C_{gate}} \sim \frac{g_m}{2\pi C_i W\,(L+2L_C)}$$

$$\sim \frac{\mu_{eff}\, V_{DS}}{2\pi L\,(L+2L_C)} \qquad \text{| linear regime}$$

$$\sim \frac{\mu_{eff}\, V_{GS}-V_{th}}{2\pi L\,(L+2L_C)} \qquad \text{| saturation regime}$$

where f_T is the cutoff frequency, g_m is the transconductance, C_i is the gate-dielectric capacitance per unit area, L is the channel length, and L_C is the gate-to-contact overlap.

Therefore, reducing the channel length always benefits the dynamic transistor performance, even if it comes at the expense of a smaller effective carrier mobility (see Figure 5).

The relationships between the lateral transistor dimensions (L, L_C) and the dynamic performance (f_T) is described in detail in references [37] and [S3].

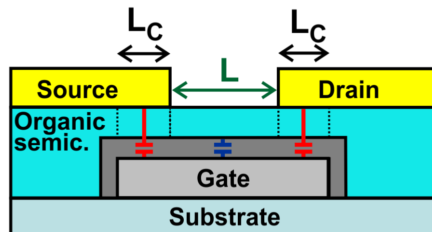

[S1] C. S. Chiang, S. Martin, J. Kanicki, Y. Ugai, T. Yukawa, S. Takeuchi, *Jpn. J. Appl. Phys.*, **1998**, *Part 1 37*, 5914
[S2] T. J. Richards, H. Sirringhaus, *J. Appl. Phys.*, **2007**, *102*, 94510-1
[S3] H. Klauk, *Chem. Soc. Rev.*, **2010**, *39*, 2643